
MOFO: MOtion FOcused Self-Supervision for Video Understanding

4th Workshop on Self-Supervised Learning: Theory and Practice
Anonymous Author(s)

Abstract

1 Self-supervised learning (SSL) techniques have recently produced outstanding re-
2 sults in learning visual representations from unlabeled videos. However, despite
3 the importance of motion in supervised learning techniques for action recognition,
4 SSL methods often do not explicitly consider motion information in videos. To
5 address this issue, we propose MOFO (MOtion FOcused), a novel SSL method for
6 focusing representation learning on the motion area of a video for action recogni-
7 tion. MOFO automatically detects motion areas in videos and uses these to guide
8 the self-supervision task. We use a masked autoencoder that randomly masks out
9 a high proportion of the input sequence and forces a specified percentage of the
10 inside of the motion area to be masked and the remainder from outside. We fur-
11 ther incorporate motion information into the finetuning step to emphasise motion
12 in the downstream task. We demonstrate that our motion-focused innovations can
13 significantly boost the performance of the currently leading SSL method (Video-
14 MAE) for action recognition. Our proposed approach significantly improves the
15 performance of the current SSL method for action recognition, indicating the im-
16 portance of explicitly encoding motion in SSL.

17

1 Introduction

18 Action recognition is an essential task in video understanding and has been extensively investigated
19 in recent years Liu et al. [2022], Wei et al. [2022], Girdhar et al. [2022a]. In video action recognition,
20 supervised deep learning techniques have made significant progress Tran et al. [2015], Feichtenhofer
21 et al. [2019], Lin et al. [2019]; However, due to the lack of labels, which must be manually collected,
22 learning to recognise actions from a small number of labelled videos is a difficult task as data collec-
23 tion will be expensive and challenging. It is especially inappropriate for long-tail open vocabulary
24 object distributions across scenes, such as a kitchen. Furthermore, getting annotations for videos is
25 much more difficult due to the large number of frames and the temporal boundaries of when actions
26 begin and end.

27 Supervised methods Wang and Gupta [2018], Kwon et al. [2020], Patrick et al. [2021] have recog-
28 nised the importance of motion to understand actions because often, key objects are moving in
29 the scene. However, most SSL methods do not explicitly consider motion or use hand-crafted fea-
30 tures Escorcia et al. [2022], limiting their effectiveness. In SSL literature, masked autoencoder
31 models Tong et al. [2022] have been proposed to learn the underlying data distribution but without
32 directly emphasising motion autonomously. Even though this model can perform spatiotemporal
33 reasoning over content, the encoder backbone is ineffective in capturing motion representations (we
34 show this later in Fig. 2). Incorporating motion information is not trivial, especially in egocentric
35 video. The primary issue lies in the stability of the results, which can be significantly impacted
36 by camera movement. When the camera moves rapidly, static objects or background pixels exhibit
37 high movement velocities in optical flow. Several existing methods leveraged object detection to im-
38 prove egocentric video recognition Wang et al. [2020b,b], Wu et al. [2019], Ma et al. [2016], among
39 which Wu et al. [2019] also incorporate temporal contexts to help understand the ongoing action.

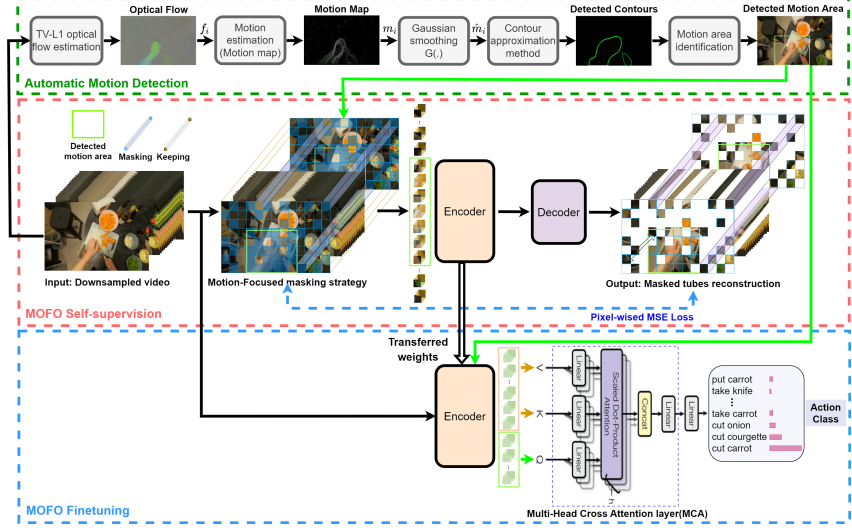


Figure 1: MOFO is a motion-focused self-supervised framework for action recognition.

40 These approaches may have limited uses in real-world systems since they demand time-consuming,
 41 labour-intensive item detection annotations and are computationally expensive. In contrast, our
 42 framework does not depend on costly object detectors.

43 Fig. 1 overviews our method, with three parts; first, our automatic motion area detection, With
 44 optical flow input to create a motion map to remove camera motion. Second, we propose our new
 45 strategy for the SSL pretext task, a reconstruction task focusing more on masking 3D patches on the
 46 motion area in the video called MOFO (Motion Focused). Thirdly, the downstream task adaptation
 47 step emphasises motion further by integrating motion information during the finetuning training. A
 48 key contribution of our work is to detect salient objects and motion in the video based on motion
 49 boundaries from optical flow. Using the motion boundaries instead of a direct optical flow output
 50 mitigates the challenge of camera motion and creates salient areas of movement or interest without
 51 a pretrained network. Given the identification of motion, we propose to provide a motion under-
 52 standing of self-supervised masking Tong et al. [2022] of 3D patches in the video frames. A further
 53 contribution is that, during the finetuning stage, MOFO prioritises the motion areas in video data
 54 identified as a self-supervision pretext task. Since motion areas contain more information, such
 55 as moving objects, actions, and interactions, our proposed model gives them a higher priority by
 56 emphasising the masking strategy to be more in the motion area.

57 2 Motion-focused Self-supervised Video Understanding

58 2.1 Automatic Motion Area Detection

59 To identify the motion areas without pretrained object detectors, we propose using classical com-
 60 puter vision features, Optical flow vectors; however, these vectors will be affected by camera motion
 61 with static objects or background pixels exhibiting high movement velocities in optical flow
 62 when the camera moves rapidly. To mitigate the problem above, we calculate the motion bound-
 63aries Dalal et al. [2006] and use these to define a motion map Li et al. [2021]. Therefore, given a
 64 video with T frames and a $H \times W$ dimension, we first extract the optical flow vectors representing
 65 $\{f_i \in \mathbb{R}^{H \times W}\}_{i=1}^T$ pixel-level motion between two consecutive frames in a video using the TV-L1
 66 algorithm Zach et al. [2007] that offers increased robustness against illumination changes, occlu-
 67 sions and noise. Then, given the horizontal and vertical displacements of each pixel between the
 68 i th frame and the $(i+1)$ th frame represented by the flow maps $u_i, v_i \in \mathbb{R}^{H \times W}$, any kind of local
 69 differential or flow difference cancels out most of the effects of the camera rotation. The resulting
 70 motion map is defined as:

$$m_i = \sqrt{(\frac{\partial u_i}{\partial x})^2 + (\frac{\partial u_i}{\partial y})^2 + (\frac{\partial v_i}{\partial x})^2 + (\frac{\partial v_i}{\partial y})^2} \quad (1)$$

71 where every component denotes the corresponding x - and y -derivative differential flow frames con-
72 tributing towards computing m_i , representing moving velocity in the i -th frame while ignoring the
73 camera motion. As a result, $m_i \in \mathbb{R}^{H \times W}$ is less influenced by camera motion and considers the
74 moving salients in the i -th frame. A low-pass Gaussian filter is used to smooth areas of the image
75 with high-frequency components to further reduce the unwanted noise effect. The Gaussian Smooth-
76 ing Operator computes an average of the surrounding pixels weighted according to the Gaussian
77 distribution (G).

78 After noise reduction, the next step is to find the boundaries of the motion. To do so, we create
79 contours Suzuki et al. [1985], which are short curves that connect points of the same hue or intensity.
80 We select the two most significant contours in each frame to create a mask that indicates the motion
81 area in a frame of a specific video. The main reason for choosing two contours is that in our datasets,
82 an action is defined by hands and the corresponding object. We create a bounding box around
83 the resulting area that precisely represents the motion in each video. In Fig. 7(a), we qualitatively
84 compare our automatic box predictions and the provided supervised annotation for Epic-Kitchens-
85 100 for several sample frames and provide further examples in the Appendix.

86 2.2 Motion-focused Self-Supervised Learning

87 MOFO uses 3D tube volume embeddings for the self-supervised pretext stage to obtain 3D video
88 patches from frames as inputs. It encodes these with a vanilla ViT Dosovitskiy et al. [2020] with
89 joint space-time attention as a backbone. We segmented each video into N non-overlapping tubes
90 $\mathbf{p}_i \in \mathbb{R}^{H_t \times W_t \times T_t}$. Then, we use a high-ratio tube masking approach to perform masked autoencoder
91 (MAE) pretraining with an asymmetric transformer-based encoder-decoder architecture reconstruc-
92 tion task. Unlike other random masking methods, we explicitly integrate the motion information
93 computed in subsection 2.1 into our masking strategy, resulting in a motion-guided approach to
94 encode motion for our MAE. Our novel tube masking strategy enforces a mask to be allied on a
95 high portion of the tubes inside the motion area. In other words, a fixed percentage of the tubes
96 (generally 75%) inside the motion area is always randomly masked to ensure the model is attend-
97 ing more to the motion area at reconstruction time. Therefore, we apply an extremely high ratio
98 masking at random (90%) while always masking a fixed percentage of the tubes (75%) inside the
99 motion area. The encoder produces a latent feature representation of the video using input frames
100 with blacked-out regions. The decoder uses the latent feature representation from the encoder. It
101 estimates the missing region using the mean squared error (MSE) loss, computed in pixel space be-
102 tween the masked patches and trained reconstructed outputs. Our design encourages the network to
103 capture more useful spatiotemporal structures, making MOFO a more meaningful task and improv-
104 ing the performance of self-supervised pretraining. All models only use the unlabelled data in the
105 training set of each dataset for pertaining.

106 2.3 Motion-focused Finetuning

107 Recall that the self-supervised learning protocol is split between a pretraining and finetuning stage.
108 We propose a new approach to focus on the motion area at both the pretext and the finetuning of
109 the model. The model is trained end-to-end during finetuning, using the weights of the pretrained
110 network as initialisation for the downstream supervised task dataset.

111 As the area inside the motion box has more semantic motion information, we wish to exploit this
112 information for our task by leveraging the detected motion box. On the other hand, the video’s
113 setting and any nearby items could provide context for categorising the video clips for the action
114 recognition task. For instance, in the case of washing dishes, the hands can be seen in the sink, but
115 the dishes beside the sink may indicate that the person is washing them. Therefore, we propose to use
116 multi-cross attention (MCA) Nagrani et al. [2021] in our encoder. MCA is an attention mechanism
117 that mixes two different embedding sequences; the two are from the same modality. Unlike self-
118 attention, where inputs are the same set, during cross-attention, they differ; MCA’s main objective
119 is to determine attention scores using data from various information sources. This module resides
120 between the encoder and MLP classifier layers, takes the inner and outer motion box embeddings,
121 and outputs the fused embedding (see details in Appendix B).

122 3 Experiments

123 We use two well-known and large datasets to evaluate our proposed approach: **Something-**
124 **Something V2 (SSV2)** Goyal et al. [2017] and **Epic-Kitchens-100** Damen et al. [2022]. Using

Table 1: Human activity recognition on **Epic-Kitchens** and **Something-Something V2 (SSV2)** in terms of Top-1 and Top-5 accuracy.

Method	Backbone	Param	SSV2		Epic-Kitchens		
			Action Top-1	Action Top-5	Verb Top-1	Noun Top-1	Action Top-1
VIMPAC Tan et al. [2021]	ViT-L	307	68.1	-	-	-	-
BEVT Wang et al. [2022]	Swin-B	88	70.6	-	-	-	-
VideoMAE Tong et al. [2022]	ViT-B	87	70.8	92.4	71.6	66.0	53.2
ST-MAE Feichtenhofer et al. [2022]	ViT-L	304	72.1	-	-	-	-
OmniMAE Girdhar et al. [2022a]	ViT-B	87	69.5	-	-	-	39.3
Omnivore(Swin-B) Girdhar et al. [2022b]	ViT-B	-	71.4	93.5	69.5	61.7	49.9
MOFO (Proposed)	ViT-B	102	75.5	95.3	74.2	68.1	54.5

125 egocentric videos to predict first-person activity faces many challenges, including a limited field of
 126 view, occlusions, and unstable motions, and there is a relative scarcity of labelled data.

127 **Results and analysis** We finetune the learnt model for action classification based on our proposed
 128 MOFO finetuning approach to evaluate the learned model as a pretrained model and train on a new
 129 downstream task with the learned representation. The entire feature encoder and a linear layer are
 130 finetuned end-to-end with cross-entropy loss, with recognition accuracy reported in Table 3. We
 131 demonstrate significant performance improvement over the other self-supervised approaches, in-
 132 creasing 2.6%, 2.1%, and 1.3% accuracy over the best-performing methods on Epic-Kitchens verb,
 133 noun and action classification and 4.7% on Something Something V2 action classification, respec-
 134 tively. In terms of masking ratio, variants are presented in the Appendix, but we found that the 75%
 135 inside masking ratio worked the best. Our strategy outperforms approaches like OmniMAE Gird-
 136 har et al. [2022a], trained jointly on images and videos by 3.2% in Top-1 accuracy. On Something
 137 Something V2, our method outperforms VIMPAC Tan et al. [2021] and ST-MAE Feichtenhofer
 138 et al. [2022], which both use ViT-Large as a backbone, whereas our backbone is vanilla ViT-Base
 139 with over 3x fewer parameters. Compared to VideoMAE Tong et al. [2022], our approach achieves
 140 significantly better results while the number of backbone parameters remains the same.

141 **Visualizing self-supervised representation**

142 To further understand the representations learnt
 143 by MOFO, we utilise GradCAM Selvaraju et al.
 144 [2017] to create a saliency map highlighting
 145 each pixel’s importance to show how each pixel
 146 contributes to the discrimination of the video
 147 clip. Fig. 2 visualises the middle frame of a
 148 video clip, the motion map of the VideoMAE
 149 and our MOFO from the fifth attention layer of
 150 the ViT-Base backbone. It is interesting to note
 151 that for similar actions: *knead dough*, *cut car-*
 152 *rot*, and *cut-in tomato*, MOFO is sensitive to the
 153 location that is the most significant motion loca-
 154 tion as detected by our automatic algorithm.

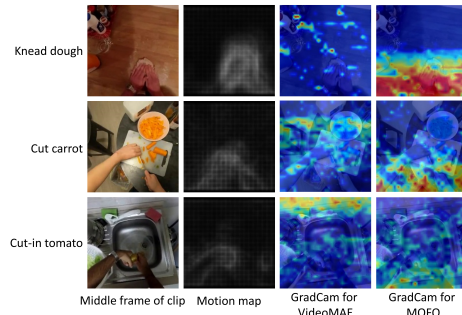


Figure 2: Visualisation of the learnt features

155 **4 Conclusion**

156 MOFO introduces a Motion-Focused technique,
 157 which explores the motion information for enhancing motion-aware self-supervised video action
 158 recognition. We propose an innovative strategy, an effective self-supervised pretext task, and a mod-
 159 ification to masked autoencoding, which focuses masking on the motion area in the video (Motion
 160 Focused). Extensive experiments on two challenging datasets demonstrate that this context-based
 161 SSL technique improves performance in action recognition tasks, and the public code will guide
 162 many research directions.

163 **References**

- 164 Arif Akar, Ufuk Umut Senturk, and Nazli Ikitzler-Cinbis. MAC: mask-augmentation for motion-
 165 aware video representation learning. In *BMVC*, 2022.

- 166 Anurag Arnab, Mostafa Dehghani, Georg Heigold, Chen Sun, Mario Lučić, and Cordelia Schmid.
167 Vivit: A video vision transformer. In *ICCV*, 2021.
- 168 Federico Baldassarre and Hossein Azizpour. Towards self-supervised learning of global and object-
169 centric representations. *arXiv preprint arXiv:2203.05997*, 2022.
- 170 Gedas Bertasius, Heng Wang, and Lorenzo Torresani. Is space-time attention all you need for video
171 understanding? In *ICML*, 2021.
- 172 Mathilde Caron, Hugo Touvron, Ishan Misra, Hervé Jégou, Julien Mairal, Piotr Bojanowski, and
173 Armand Joulin. Emerging properties in self-supervised vision transformers. In *ICCV*, 2021.
- 174 Joao Carreira and Andrew Zisserman. Quo vadis, action recognition? a new model and the kinetics
175 dataset. In *CVPR*, 2017.
- 176 Ting Chen, Simon Kornblith, Kevin Swersky, Mohammad Norouzi, and Geoffrey E. Hinton. Big
177 self-supervised models are strong semi-supervised learners. In *NeurIPS*, 2020.
- 178 Yabo Chen, Yuchen Liu, Dongsheng Jiang, Xiaopeng Zhang, Wenrui Dai, Hongkai Xiong, and
179 Qi Tian. Sdae: Self-distilled masked autoencoder. In *ECCV*, 2022.
- 180 Subhabrata Choudhury, Laurynas Karazija, Iro Laina, Andrea Vedaldi, and Christian Rupprecht.
181 Guess what moves: Unsupervised video and image segmentation by anticipating motion. *BMVC*,
182 2022.
- 183 Navneet Dalal, Bill Triggs, and Cordelia Schmid. Human detection using oriented histograms of
184 flow and appearance. In *ECCV*, 2006.
- 185 Dima Damen, Hazel Doughty, Giovanni Maria Farinella, Sanja Fidler, Antonino Furnari, Evangelos
186 Kazakos, Davide Moltisanti, Jonathan Munro, Toby Perrett, Will Price, et al. Scaling egocentric
187 vision: The epic-kitchens dataset. In *ECCV*, 2018.
- 188 Dima Damen, Hazel Doughty, Giovanni Maria Farinella, Sanja Fidler, Antonino Furnari, Evangelos
189 Kazakos, Davide Moltisanti, Jonathan Munro, Toby Perrett, Will Price, et al. The epic-kitchens
190 dataset: Collection, challenges and baselines. *IEEE Transactions on Pattern Analysis and Ma-*
191 *chine Intelligence*, 2020a.
- 192 Dima Damen, Hazel Doughty, Giovanni Maria Farinella, Antonino Furnari, Evangelos Kazakos,
193 Jian Ma, Davide Moltisanti, Jonathan Munro, Toby Perrett, Will Price, et al. Rescaling egocentric
194 vision. *arXiv preprint arXiv:2006.13256*, 2020b.
- 195 Dima Damen, Hazel Doughty, Giovanni Maria Farinella, Antonino Furnari, Evangelos Kazakos,
196 Jian Ma, Davide Moltisanti, Jonathan Munro, Toby Perrett, Will Price, et al. Rescaling egocentric
197 vision: Collection, pipeline and challenges for epic-kitchens-100. *IJCV*, 2022.
- 198 Jacob Devlin, Ming-Wei Chang, Kenton Lee, and Kristina Toutanova. Bert: Pre-training of deep
199 bidirectional transformers for language understanding. *arXiv preprint arXiv:1810.04805*, 2018.
- 200 Jacob Devlin, Ming-Wei Chang, Kenton Lee, and Kristina Toutanova. BERT: pre-training of deep
201 bidirectional transformers for language understanding. In *NAACL*, pages 4171–4186, 2019.
- 202 Carl Doersch, Abhinav Gupta, and Alexei A Efros. Unsupervised visual representation learning by
203 context prediction. In *ICCV*, pages 1422–1430, 2015.
- 204 Jeffrey Donahue, Lisa Anne Hendricks, Sergio Guadarrama, Marcus Rohrbach, Subhashini Venu-
205 gopalan, Kate Saenko, and Trevor Darrell. Long-term recurrent convolutional networks for visual
206 recognition and description. In *CVPR*, 2015.
- 207 Alexey Dosovitskiy, Lucas Beyer, Alexander Kolesnikov, Dirk Weissenborn, Xiaohua Zhai, Thomas
208 Unterthiner, Mostafa Dehghani, Matthias Minderer, Georg Heigold, Sylvain Gelly, et al. An
209 image is worth 16x16 words: Transformers for image recognition at scale. *ICLR*, 2020.
- 210 Victor Escorcia, Ricardo Guerrero, Xiatian Zhu, and Brais Martinez. Sos! self-supervised learning
211 over sets of handled objects in egocentric action recognition. In *ECCV*, 2022.

- 212 Haoqi Fan, Bo Xiong, Karttikeya Mangalam, Yanghao Li, Zhicheng Yan, Jitendra Malik, and
213 Christoph Feichtenhofer. Multiscale vision transformers. In *ICCV*, 2021.
- 214 Christoph Feichtenhofer, Axel Pinz, and Richard P Wildes. Spatiotemporal multiplier networks for
215 video action recognition. In *CVPR*, 2017.
- 216 Christoph Feichtenhofer, Haoqi Fan, Jitendra Malik, and Kaiming He. Slowfast networks for video
217 recognition. In *ICCV*, 2019.
- 218 Christoph Feichtenhofer, haoqi fan, Yanghao Li, and Kaiming He. Masked autoencoders as spa-
219 tiotemporal learners. In *NeurIPS*, 2022.
- 220 Basura Fernando, Hakan Bilen, Efstratios Gavves, and Stephen Gould. Self-supervised video repre-
221 sentation learning with odd-one-out networks. In *CVPR*, 2017.
- 222 David J. Fleet and Allan D. Jepson. Stability of phase information. *IEEE TPAMI*, 1993.
- 223 Valentin Gabeur, Chen Sun, Karteek Alahari, and Cordelia Schmid. Multi-modal transformer for
224 video retrieval. In *ECCV*, 2020.
- 225 Rohit Girdhar, Alaaeldin El-Nouby, Mannat Singh, Kalyan Vasudev Alwala, Armand Joulin, and
226 Ishan Misra. Omnimae: Single model masked pretraining on images and videos. *arXiv preprint*
227 *arXiv:2206.08356*, 2022a.
- 228 Rohit Girdhar, Mannat Singh, Nikhila Ravi, Laurens van der Maaten, Armand Joulin, and Ishan
229 Misra. Omnivore: A single model for many visual modalities. In *CVPR*, 2022b.
- 230 Raghav Goyal, Samira Ebrahimi Kahou, Vincent Michalski, Joanna Materzynska, Susanne West-
231 phal, Heuna Kim, Valentin Haenel, Ingo Fruend, Peter Yianilos, Moritz Mueller-Freitag, et al.
232 The "something something" video database for learning and evaluating visual common sense. In
233 *ICCV*, 2017.
- 234 Sheng Guo, Zihua Xiong, Yujie Zhong, Limin Wang, Xiaobo Guo, Bing Han, and Weilin Huang.
235 Cross-architecture self-supervised video representation learning. In *CVPR*, 2022.
- 236 Agrim Gupta, Stephen Tian, Yunzhi Zhang, Jiajun Wu, Roberto Martín-Martín, and Li Fei-Fei.
237 Maskvit: Masked visual pre-training for video prediction. *arXiv preprint arXiv:2206.11894*,
238 2022.
- 239 Kaiming He, Xinlei Chen, Saining Xie, Yanghao Li, Piotr Dollár, and Ross Girshick. Masked
240 autoencoders are scalable vision learners. In *CVPR*, 2022.
- 241 Andrej Karpathy, George Toderici, Sanketh Shetty, Thomas Leung, Rahul Sukthankar, and Li Fei-
242 Fei. Large-scale video classification with convolutional neural networks. In *CVPR*, 2014.
- 243 Muhammad Attique Khan, Kashif Javed, Sajid Ali Khan, Tanzila Saba, Usman Habib, Junaid Ali
244 Khan, and Aaqif Afzaal Abbasi. Human action recognition using fusion of multiview and deep
245 features: an application to video surveillance. *Multimedia tools and applications*, 2020.
- 246 Salman Khan, Muzammal Naseer, Munawar Hayat, Syed Waqas Zamir, Fahad Shahbaz Khan, and
247 Mubarak Shah. Transformers in vision: A survey. *ACM computing surveys (CSUR)*, 2022.
- 248 Heeseung Kwon, Manjin Kim, Suha Kwak, and Minsu Cho. Motionsqueeze: Neural motion feature
249 learning for video understanding. In *ECCV*, 2020.
- 250 Conglong Li, Zhewei Yao, Xiaoxia Wu, Minjia Zhang, and Yuxiong He. Deepspeed data efficiency:
251 Improving deep learning model quality and training efficiency via efficient data sampling and
252 routing. *arXiv preprint arXiv:2212.03597*, 2022a.
- 253 Gang Li, Heliang Zheng, Daqing Liu, Chaoyue Wang, Bing Su, and Changwen Zheng. Semmae:
254 Semantic-guided masking for learning masked autoencoders. *NeurIPS*, 2022b.
- 255 Haofeng Li, Guanqi Chen, Guanbin Li, and Yizhou Yu. Motion guided attention for video salient
256 object detection. In *ICCV*, 2019.

- 257 Rui Li, Yiheng Zhang, Zhaofan Qiu, Ting Yao, Dong Liu, and Tao Mei. Motion-focused contrastive
258 learning of video representations. In *ICCV*, 2021.
- 259 Yanghao Li, Chao-Yuan Wu, Haoqi Fan, Karttikeya Mangalam, Bo Xiong, Jitendra Malik, and
260 Christoph Feichtenhofer. Mvity2: Improved multiscale vision transformers for classification and
261 detection. In *CVPR*, 2022c.
- 262 Ji Lin, Chuang Gan, and Song Han. Tsm: Temporal shift module for efficient video understanding.
263 In *ICCV*, 2019.
- 264 Ze Liu, Jia Ning, Yue Cao, Yixuan Wei, Zheng Zhang, Stephen Lin, and Han Hu. Video swin
265 transformer. In *CVPR*, June 2022.
- 266 Jonathon Luiten, Idil Esen Zulfikar, and Bastian Leibe. Unovost: Unsupervised offline video object
267 segmentation and tracking. In *WACV*, 2020.
- 268 Minghuang Ma, Haoqi Fan, and Kris M Kitani. Going deeper into first-person activity recognition.
269 In *CVPR*, 2016.
- 270 Joanna Materzynska, Tete Xiao, Roei Herzig, Huijuan Xu, Xiaolong Wang, and Trevor Darrell.
271 Something-else: Compositional action recognition with spatial-temporal interaction networks. In
272 *CVPR*, 2020.
- 273 Arsha Nagrani, Shan Yang, Anurag Arnab, Aren Jansen, Cordelia Schmid, and Chen Sun. Attention
274 bottlenecks for multimodal fusion. *NeurIPS*, 2021.
- 275 Mehdi Noroozi and Paolo Favaro. Unsupervised learning of visual representations by solving jigsaw
276 puzzles. In *ECCV*, 2016.
- 277 Adrián Núñez-Marcos, Gorka Azkune, and Ignacio Arganda-Carreras. Egocentric vision-based
278 action recognition: A survey. *Neurocomputing*, 2022.
- 279 Deepak Pathak, Philipp Krahenbuhl, Jeff Donahue, Trevor Darrell, and Alexei A Efros. Context
280 encoders: Feature learning by inpainting. In *CVPR*, 2016.
- 281 Mandela Patrick, Dylan Campbell, Yuki Asano, Ishan Misra, Florian Metze, Christoph Feichten-
282 hofer, Andrea Vedaldi, and Joao F Henriques. Keeping your eye on the ball: Trajectory attention
283 in video transformers. *NeurIPS*, 2021.
- 284 Tomas Pfister, James Charles, and Andrew Zisserman. Flowing convnets for human pose estimation
285 in videos. In *Proceedings of the IEEE international conference on computer vision*, 2015.
- 286 Sudeep Sarkar, P Jonathon Phillips, Zongyi Liu, Isidro Robledo Vega, Patrick Grother, and Kevin W
287 Bowyer. The humanoid gait challenge problem: Data sets, performance, and analysis. *IEEE*
288 *transactions on pattern analysis and machine intelligence*, 2005.
- 289 Ramprasaath R Selvaraju, Michael Cogswell, Abhishek Das, Ramakrishna Vedantam, Devi Parikh,
290 and Dhruv Batra. Grad-cam: Visual explanations from deep networks via gradient-based local-
291 ization. In *ICCV*, 2017.
- 292 Ufuk Umut Senturk, Arif Akar, and Nazli Ikizler-Cinbis. Triplednet: Exploring depth estimation
293 with self-supervised representation learning. 2022.
- 294 A H. Shabani, J S. Zelek, and D A. Clausi. Robust local video event detection for action recognition.
295 In *NeurIPS, Machine Learning for Assistive Technology Workshop*, 2010.
- 296 Amir Hossein Shabani, David A Clausi, and John S Zelek. Improved spatio-temporal salient feature
297 detection for action recognition. In *BMVC*, 2011.
- 298 Dandan Shan, Jiaqi Geng, Michelle Shu, and David F Fouhey. Understanding human hands in
299 contact at internet scale. In *CVPR*, 2020.
- 300 Hedvig Sidenbladh, Michael J Black, and David J Fleet. Stochastic tracking of 3d human figures
301 using 2d image motion. In *ECCV*, 2000.

- 302 Karen Simonyan and Andrew Zisserman. Two-stream convolutional networks for action recognition
303 in videos. *NeurIPS*, 2014.
- 304 S Sowmyayani and P Arockia Jansi Rani. Stharnet: Spatio-temporal human action recognition
305 network in content based video retrieval. *Multimedia Tools and Applications*, 2022.
- 306 Satoshi Suzuki et al. Topological structural analysis of digitized binary images by border following.
307 *Computer vision, graphics, and image processing*, 1985.
- 308 Hao Tan, Jie Lei, Thomas Wolf, and Mohit Bansal. Vimpac: Video pre-training via masked token
309 prediction and contrastive learning. *arXiv preprint arXiv:2106.11250*, 2021.
- 310 Zhan Tong, Yibing Song, Jue Wang, and Limin Wang. Videomae: Masked autoencoders are data-
311 efficient learners for self-supervised video pre-training. *NeurIPS*, 2022.
- 312 Du Tran, Lubomir Bourdev, Rob Fergus, Lorenzo Torresani, and Manohar Paluri. Learning spa-
313 tiotemporal features with 3d convolutional networks. In *ICCV*, 2015.
- 314 GÜl Varol, Ivan Laptev, and Cordelia Schmid. Long-term temporal convolutions for action recogni-
315 tion. *TPAMI*, 2017.
- 316 Ashish Vaswani, Noam Shazeer, Niki Parmar, Jakob Uszkoreit, Llion Jones, Aidan N Gomez,
317 Łukasz Kaiser, and Illia Polosukhin. Attention is all you need. *NeurIPS*, 2017.
- 318 Namrata Vaswani, Amit K Roy-Chowdhury, and Rama Chellappa. " shape activity": a continuous-
319 state hmm for moving/deforming shapes with application to abnormal activity detection. *IEEE*
320 *Transactions on Image Processing*, 2005.
- 321 Paul Viola, Michael J Jones, and Daniel Snow. Detecting pedestrians using patterns of motion and
322 appearance. *IJCV*, 2005.
- 323 Jiangliu Wang, Jianbo Jiao, Linchao Bao, Shengfeng He, Yunhui Liu, and Wei Liu. Self-supervised
324 spatio-temporal representation learning for videos by predicting motion and appearance statistics.
325 In *CVPR*, 2019.
- 326 Jiangliu Wang, Jianbo Jiao, and Yun-Hui Liu. Self-supervised video representation learning by pace
327 prediction. In *ECCV*, 2020a.
- 328 Lei Wang and Piotr Koniusz. Self-supervising action recognition by statistical moment and subspace
329 descriptors. In *ACMMM*, 2021.
- 330 Limin Wang, Zhan Tong, Bin Ji, and Gangshan Wu. Tdn: Temporal difference networks for efficient
331 action recognition. In *CVPR*, 2021.
- 332 Rui Wang, Dongdong Chen, Zuxuan Wu, Yinpeng Chen, Xiyang Dai, Mengchen Liu, Yu-Gang
333 Jiang, Luowei Zhou, and Lu Yuan. Bevt: Bert pretraining of video transformers. In *CVPR*, 2022.
- 334 Xiaohan Wang, Yu Wu, Linchao Zhu, and Yi Yang. Symbiotic attention with privileged information
335 for egocentric action recognition. In *AAAI*, 2020b.
- 336 Xiaolong Wang and Abhinav Gupta. Videos as space-time region graphs. In *ECCV*, 2018.
- 337 Chen Wei, Haoqi Fan, Saining Xie, Chao-Yuan Wu, Alan Yuille, and Christoph Feichtenhofer.
338 Masked feature prediction for self-supervised visual pre-training. In *CVPR*, 2022.
- 339 Chao-Yuan Wu, Christoph Feichtenhofer, Haoqi Fan, Kaiming He, Philipp Krahenbuhl, and Ross
340 Girshick. Long-term feature banks for detailed video understanding. In *CVPR*, 2019.
- 341 Qizhe Xie, Minh-Thang Luong, Eduard Hovy, and Quoc V Le. Self-training with noisy student
342 improves imagenet classification. In *CVPR*, 2020.
- 343 Xuehan Xiong, Anurag Arnab, Arsha Nagrani, and Cordelia Schmid. M&m mix: A multimodal
344 multiview transformer ensemble. *arXiv preprint arXiv:2206.09852*, 2022.
- 345 Yuwen Xiong, Mengye Ren, Wenyuan Zeng, and Raquel Urtasun. Self-supervised representation
346 learning from flow equivariance. In *ICCV*, 2021.

- 347 Dejing Xu, Jun Xiao, Zhou Zhao, Jian Shao, Di Xie, and Yueting Zhuang. Self-supervised spa-
 348 tiotemporal learning via video clip order prediction. In *CVPR*, 2019.
- 349 Shen Yan, Xuehan Xiong, Anurag Arnab, Zhichao Lu, Mi Zhang, Chen Sun, and Cordelia Schmid.
 350 Multiview transformers for video recognition. In *CVPR*, 2022.
- 351 Charig Yang, Hala Lamdouar, Erika Lu, Andrew Zisserman, and Weidi Xie. Self-supervised video
 352 object segmentation by motion grouping. In *ICCV*, 2021.
- 353 Xitong Yang, Xiaodong Yang, Sifei Liu, Deqing Sun, Larry Davis, and Jan Kautz. Hierarchical
 354 contrastive motion learning for video action recognition. *arXiv preprint arXiv:2007.10321*, 2020.
- 355 Sukmin Yun, Hankook Lee, Jaehyung Kim, and Jinwoo Shin. Patch-level representation learning
 356 for self-supervised vision transformers. In *CVPR*, 2022.
- 357 Christopher Zach, Thomas Pock, and Horst Bischof. A duality based approach for realtime tv-l 1
 358 optical flow. In *Pattern Recognition: 29th DAGM Symposium, Heidelberg, Germany, September
 359 12-14, 2007. Proceedings 29*, 2007.
- 360 Can Zhang, Yuexian Zou, Guang Chen, and Lei Gan. Pan: Persistent appearance network with an
 361 efficient motion cue for fast action recognition. In *ACMMM*, 2019.
- 362 Chuhan Zhang, Ankush Gupta, and Andrew Zisserman. Is an object-centric video representation
 363 beneficial for transfer? In *ACCV*, 2022.
- 364 Hao Zhang, Yanbin Hao, and Chong-Wah Ngo. Token shift transformer for video classification. In
 365 *ACMMM*, 2021.
- 366 Richard Zhang, Phillip Isola, and Alexei A Efros. Colorful image colorization. In *ECCV*, 2016.

367 Appendix

368 We also conducted various ablation studies to examine the design choices made in our proposed
 369 strategy.

370 A Motion-focused Self-supervised Learning

371 **Experimental setting.** MOFO uses ViT-Base as a decoder/encoder backbone, trained for 800
 372 epochs on Something-Something V2 and Epic-Kitchens for the SSL independently. We follow the
 373 training and experiential parameters from recent work Tong et al. [2022] to ensure a fair comparison
 374 and finetune for 100 epochs with early stopping. The model takes 16 frames from the video with
 375 224×224 size and divides the input video into a 3D $16 \times 16 \times 8$ patch embeddings, resulting in
 376 $H = 224$, $W = 224$, $T = 16$, $H_t = 16$, $W_t = 16$, $T_t = 8$, and $N = 392$. While we have a fixed
 377 number of input patches for our model, we do not have a fixed number of inner N_{inner} and outer
 378 N_{outer} embeddings due to varying size of the motion area in each video clip. We report Top-1 accu-
 379 racy on Epic-Kitchens and Top-1 and Top-5 accuracy on Something-Something V2 on downstream
 380 tasks and use Pytorch and DeepSpeed Li et al. [2022a] on 4xNVIDIA Quadro RTX-5000 GPU for
 381 our experiments.

382 **Masking ratio.** VideoMAE Tong et al. [2022] recommended tube masking with an extremely
 383 high ratio which helps reduce information leakage during masked modelling. They demonstrated
 384 the best efficiency and efficacy with a masking ratio of 90%. Therefore, we explore the effect of
 385 the inside masking ratio for verb classification on Epic-Kitchens in Fig. 3. It shows that the model
 386 pretrained with a masking ratio of 90% as the general masking ratio for a video and a high ratio for
 387 inside masking ratio (75%) achieves the highest efficiency level. Thus, we continue experimenting
 388 with the rest by fixing the inside mask ratio to 75%.

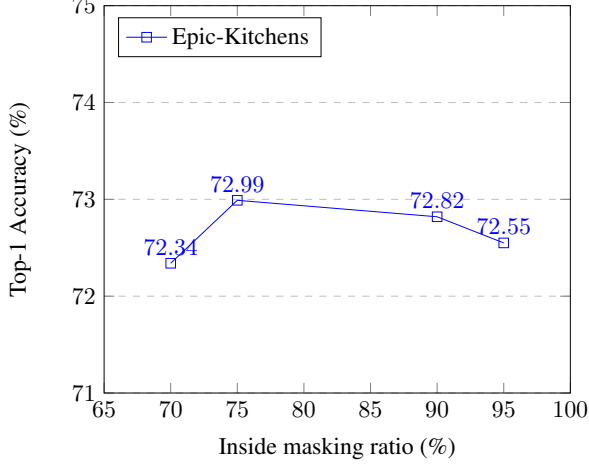


Figure 3: The effect of inside masking ratio on Epic-Kitchens-100 dataset for verb classification demonstrates that a high inside masking ratio (75%) delivers the best efficiency and effectiveness trade-off.

389 **Reconstructed frames** This section shows several reconstructed image frames from a video in
 390 Fig. 4 and Fig. 5. We use an asymmetric encoder-decoder architecture to accomplish video self-
 391 supervised pretraining tube masking with a high ratio for MAE pretraining. We can reconstruct the
 392 masked patches using random tube masking by finding the spatially and temporally corresponding
 393 unmasked patches in the adjacent frames. The loss function is the mean squared error (MSE) loss
 394 between normalised masked tokens and reconstructed tokens in pixel space. Videos are all randomly
 395 chosen from the validation sets of both datasets. Our proposed MOFO model ensures that a fixed
 396 number of masks exist within the motion area compared to the VideoMAE model. These examples
 397 suggest that, compared to VideoMAE, our MOFO model reconstructs the samples in the motion area
 398 significantly more accurately, demonstrating that the model has focused on the motion area. We can
 399 produce satisfying reconstruction results, mainly when motion occurs with our MOFO, by applying
 400 extremely high ratio masking at random (90%) while always masking a fixed percentage of the tubes
 401 (75%) inside the motion area.

402 B Motion-focused Finetuning

403 **Setup Details** Given a set of patches $\{\mathbf{p}_i\}_1^N$, the transformer yields two sets of embeddings:
 404 $\{\mathbf{e}^{\text{inner}}\}_{j=1}^{N_{\text{inner}}}$ for the inner motion boxes and $\{\mathbf{e}^{\text{outer}}\}_{k=1}^{N_{\text{outer}}}$ for the outer ones, as described by:

$$\{\mathbf{e}^{\text{inner}}\}_{j=1}^{N_{\text{inner}}}, \{\mathbf{e}^{\text{outer}}\}_{k=1}^{N_{\text{outer}}} = \text{ViT}(\{\mathbf{p}_i\}_1^N) \quad (2)$$

405 These embeddings are then processed by a cross-attention mechanism, where Q , K , and V represent
 406 query, key, and value, respectively. The CrossAttention function is formalised as follows:

$$\text{CrossAttention}(Q, K, V) = \text{softmax}\left(\frac{QK^T}{\sqrt{d_k}}\right)V \quad (3)$$

407 where $Q = \mathbf{e}^{\text{inner}}$, $K = V = \mathbf{e}^{\text{outer}}$. In the context of multi-head attention, each attention head i
 408 is computed by applying the CrossAttention function to the query, key, and value matrices, each
 409 weighted by a different learned weight matrix $W_i^Q \in \mathbb{R}^{d_{\text{model}} \times d_q}$, $W_i^K \in \mathbb{R}^{d_{\text{model}} \times d_k}$, $W_i^V \in$
 410 $\mathbb{R}^{d_{\text{model}} \times d_v}$ respectively:

$$\text{head}_i = \text{CrossAttention}(QW_i^Q, KW_i^K, VW_i^V) \quad (4)$$

411 Finally, the fused embedding $\mathbf{e}^{\text{fused}}$ is computed by concatenating the results from all attention
 412 heads and then applying another learned weight matrix $W^O \in \mathbb{R}^{hd_v \times d_{\text{model}}}$. This multi-head cross-

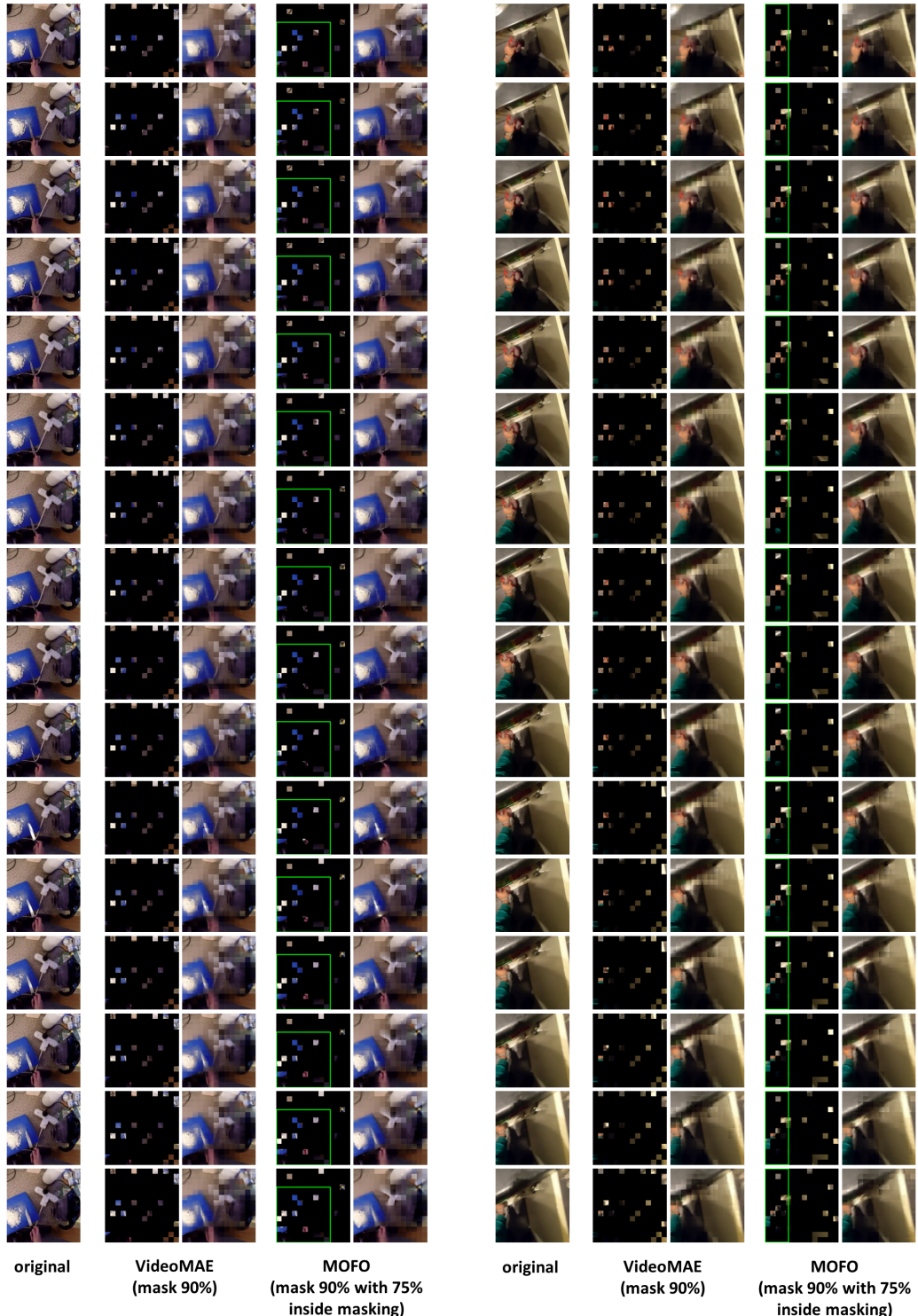


Figure 4: Qualitative Comparison on reconstructions using VideoMAE and MOFO on **Epic-Kitchens** dataset. MOFO Reconstructions of videos are predicted by MOFO pre-trained with a masking ratio of 90% and an inside masking ratio of 75% .

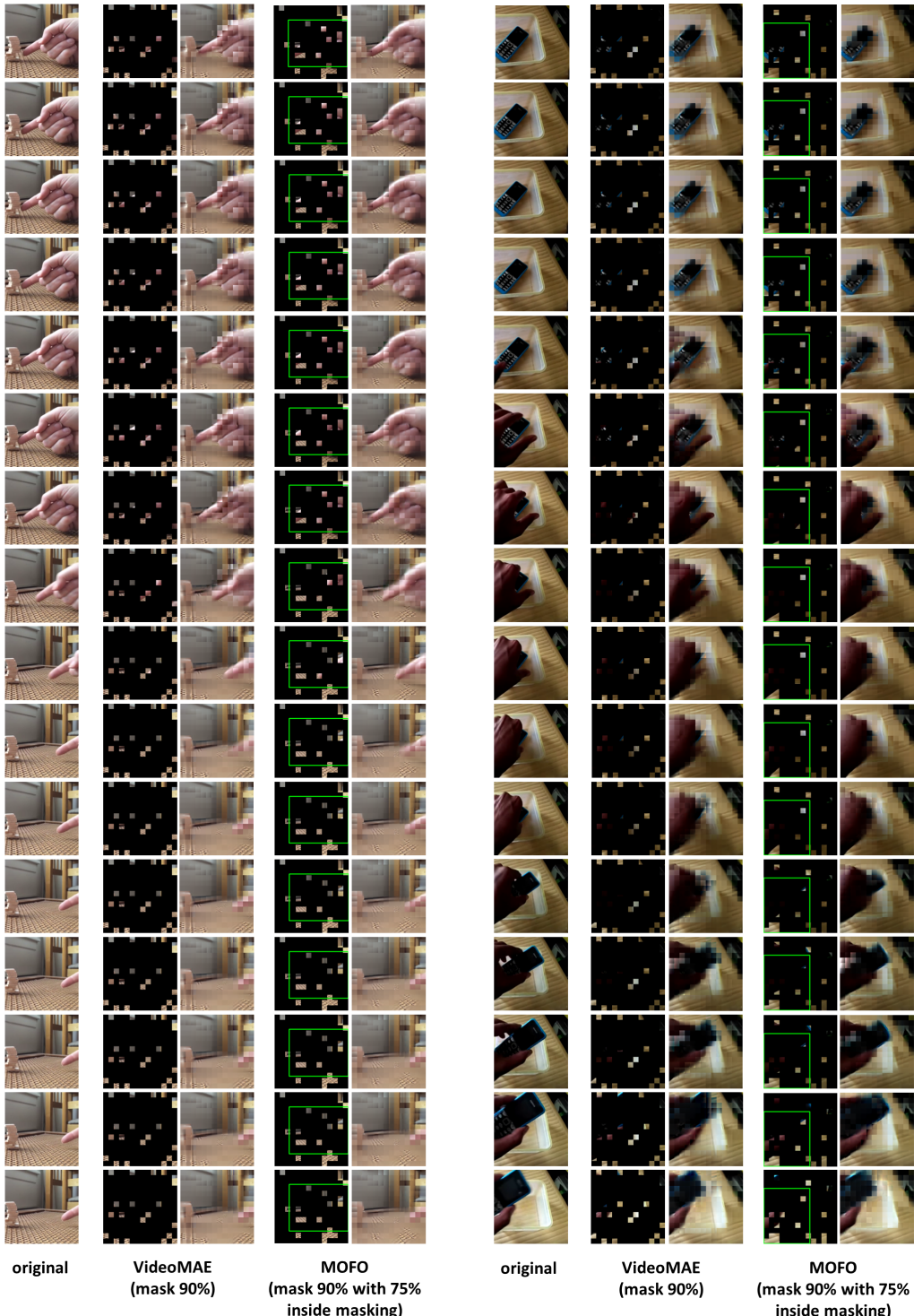


Figure 5: Qualitative Comparison on reconstructions using VideoMAE and MOFO on **Something-Something V2** dataset. MOFO Reconstructions of videos are predicted by MOFO pre-trained with a masking ratio of 90% and an inside masking ratio of 75%.

413 attention (MCA) operation can be represented as:

$$\mathbf{e}^{\text{fused}} = \text{MCA}(Q, K, V) = \text{Concat}(\text{head}_1, \dots, \text{head}_h) W^O \quad (5)$$

414 We employ $h = 3$ parallel attention layers, or heads, in this work. We also use $d_q = d_k = d_v =$
415 d_{model} for each. The model is ultimately finetuned with a cross-entropy loss \mathcal{L} :

$$\begin{aligned} \mathcal{L} &= - \sum_n \mathbf{y}_n \log \hat{\mathbf{y}}_n \\ \hat{\mathbf{y}} &= \text{FC}(\mathbf{e}^{\text{fused}}) \end{aligned} \quad (6)$$

416 where, \mathbf{y}_n is the true label for n th video clip, $\hat{\mathbf{y}}_n$ is its predicted label, and FC is the fully connected
417 layers typically used for classification.

418 **MCA hyper-parameters ablation.** We list the MCA hyperparameters used in our MOFO finetuning-
419 ing experiments here. We experiment with various head and depth settings when Epic-Kitchens is
420 the target dataset shown in Table 2. We experiment with these parameters for the verb task on Epic-
421 Kitchens to find the best choice for the cross-attention layer we suggested for MOFO finetuning.
422 The final head and depth are 3 and 1, respectively.

Table 2: Ablation experiment for number of head and depth in MOFO finetuning

Finetuning method	Backbone training	CA heads	CA depths	Epic-Kitchens Verb Top-1
VideoMAE	VideoMAE	-	-	71.6
MOFO	VideoMAE	1	1	73.5
MOFO	VideoMAE	1	2	73.8
MOFO	VideoMAE	1	3	73.6
MOFO	VideoMAE	2	1	73.7
MOFO	VideoMAE	2	2	73.3
MOFO	VideoMAE	3	1	74.0
MOFO	VideoMAE	3	2	73.5
MOFO	VideoMAE	4	1	73.8
MOFO	VideoMAE	4	2	73.3

423 **Visualisation of GradCAM using MOFO self-supervision** We visualise the GradCAM and motion-
424 map in Fig. 6 for the samples in which VideoMAE can't identify the class, but our MOFO can.
425 The attention maps show how effective our approach is in capturing the motion area. Visualisation
426 of important areas. The heatmap indicates how much the pretrained model attends to the region.

427 C Ablation Study

428 We finetune the learnt model for action classification to evaluate the learned model as a pretrained
429 model and train on a new downstream task with the learned representation. We perform such an
430 evaluation on our self-supervised model to gain some insights into the generality of the learned fea-
431 tures. For finetuning, we follow the same protocol in Tong et al. [2022] to provide a fair comparison
432 and call it regular finetuning. The entire feature encoder and a linear layer are finetuned end-to-end
433 with cross-entropy loss. The recognition accuracy for our MOFO SSL using regular finetuning is
434 reported in Table 3 shown as MOFO*. We demonstrate significant performance improvement over
435 the other self-supervised approaches, comparable to the best-supervised approach. All variants of
436 our model are presented in section A outperformed the existing result using ViT-MAE, but we
437 found that the 75% inside masking ratio worked the best. Compared to VideoMAE Tong et al.
438 [2022], our approach achieves significantly better results while the number of backbone parameters
439 remains the same. While MOFO** indicates our result with pretraining on non-motion SSL and
440 MOFO finetuning, which further increases accuracy, MOFO† denotes the MOFO SSL and MOFO
441 finetuning, which we mention in Table 3 as MOFO(Proposed), and this provides the greatest perfor-
442 mance over the best-performing methods on Epic-Kitchens verb, noun and action classification and
443 on Something Something V2 action classification.

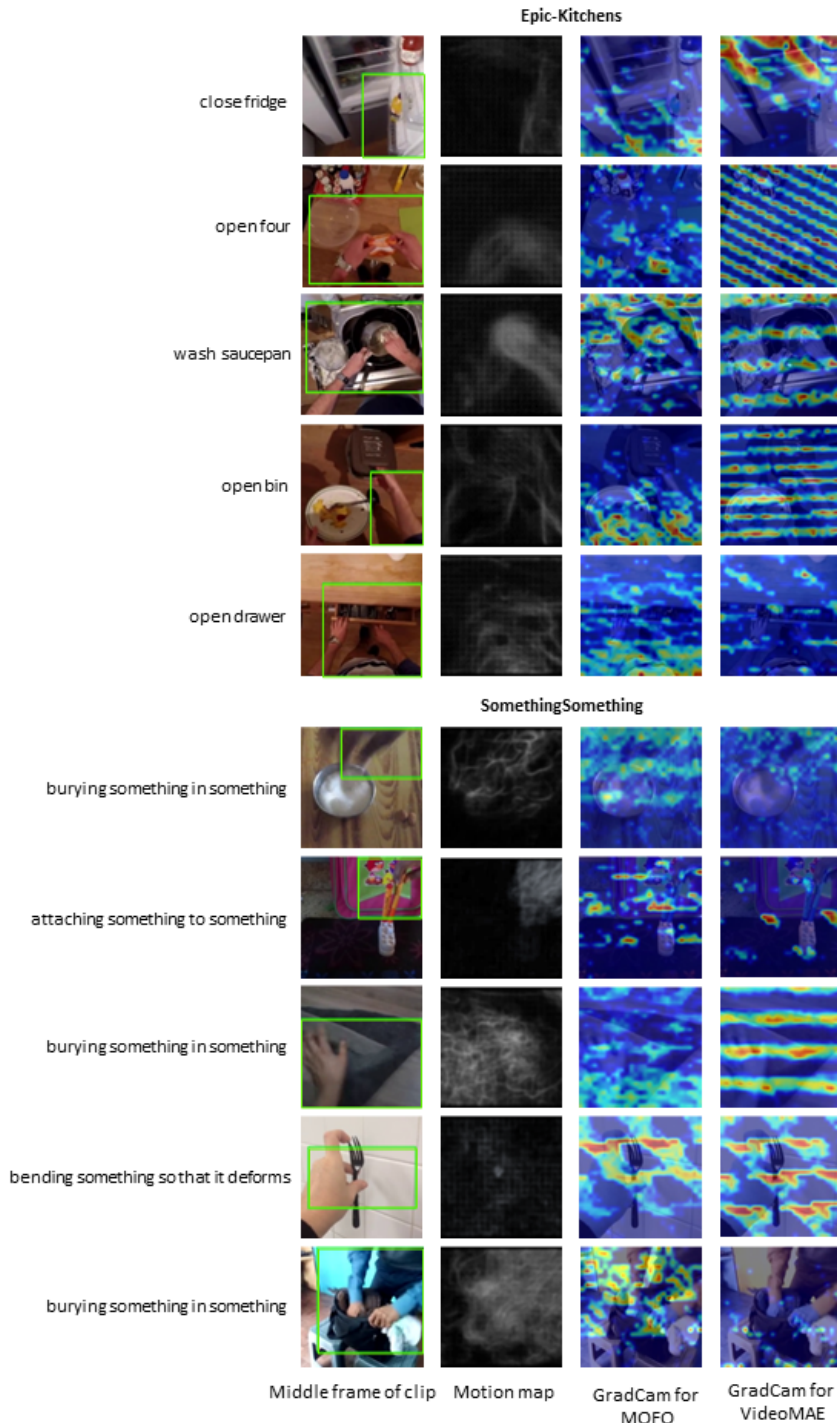


Figure 6: We visualise the attention maps generated by GradCAM based on VideoMAE and MOFO for Epic-Kitchens and the Something-Something V2 dataset. The attention maps show that our proposed approach can better capture the motion area.

Table 3: Human activity recognition on **Epic-Kitchens** and **Something-Something V2 (SSV2)** in terms of Top-1 and Top-5 accuracy. **blue:** This is the result computed by us using the public code MOFO* is pretrained by our MOFO SSL and uses non-MOFO finetuning. MOFO** This is our result with pretraining on non-MOFO SSL and has MOFO finetuning. MOFO[†] denotes the MOFO SSL and MOFO finetuning.

Method	Backbone	Param	SSV2		Epic-Kitchens		
			Action Top-1	Action Top-5	Verb Top-1	Noun Top-1	Action Top-1
<i>Supervised</i>							
TDN _{EN} Wang et al. [2021]	ResNet101@E2	88	69.6	92.2	-	-	-
SlowFast Feichtenhofer et al. [2019]	ResNet101	53	63.1	87.6	65.6	50.0	38.5
TSM Lin et al. [2019]	ResNet-50	-	63.4	88.5	67.9	49.0	38.3
MViTv1 Fan et al. [2021]	MViTv1-B	37	67.7	90.9	-	-	-
TimeSformer Bertasius et al. [2021]	ViT-B	121	59.9	-	-	-	-
TimeSformer Bertasius et al. [2021]	ViT-L	430	62.4	-	-	-	-
ViT-FE Arnab et al. [2021]	ViT-L	-	65.9	89.9	66.4	56.8	44.0
Mformer Patrick et al. [2021]	ViT-B	109	66.5	90.1	66.7	56.5	43.1
Mformer Patrick et al. [2021]	ViT-L	382	68.1	91.2	67.1	57.6	44.1
Video SWin Liu et al. [2022]	Swin-B	88	69.6	92.7	67.8	57.0	46.1
<i>Self-supervised</i>							
VIMPAC Tan et al. [2021]	ViT-L	307	68.1	-	-	-	-
BEVT Wang et al. [2022]	Swin-B	88	70.6	-	-	-	-
VideoMAE Tong et al. [2022]	ViT-B	87	70.8	92.4	71.6	66.0	53.2
ST-MAE Feichtenhofer et al. [2022]	ViT-L	304	72.1	-	-	-	-
OmniMAE Girdhar et al. [2022a]	ViT-B	87	69.5	-	-	-	39.3
Omnivore(Swin-B) Girdhar et al. [2022b]	ViT-B	-	71.4	93.5	69.5	61.7	49.9
Ours(MOFO*)	ViT-B	87	72.7	94.2	73.0	67.1	54.1
Ours(MOFO**) 	ViT-B	102	74.7	95.0	74.0	68.0	54.5
Ours(MOFO[†])	ViT-B	102	75.5	95.3	74.2	68.1	54.5

Table 4: Human activity recognition on **Epic-Kitchens** and **Something-Something V2** in terms of Top-1 accuracy. **blue:** This is the result computed by us using the public code MOFO* is pretrained by our MOFO SSL and uses non-MOFO (regular) finetuning.

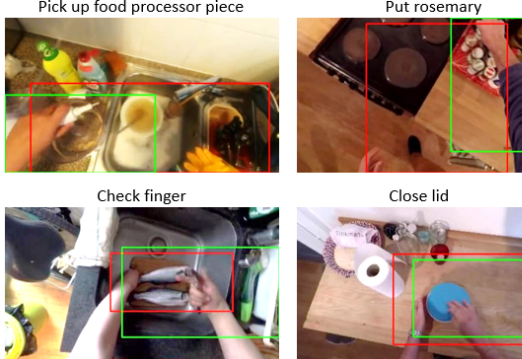
Method	Backbone	Pretrain Dataset	Something-Something V2		Epic-Kitchens		
			Action Top-1	Action Top-1	Verb Top-1	Noun Top-1	Action Top-1
VideoMAE Tong et al. [2022]	ViT-B	<i>Something – SomethingV2</i>	70.8		70.2	62.9	50.7
VideoMAE Tong et al. [2022]	ViT-B	<i>Epic – Kitchens</i>	67.3		71.6	66.0	53.2
Ours(MOFO*)	ViT-B	<i>Something – SomethingV2</i>		72.7	70.0	62.7	50.6
Ours(MOFO*)	ViT-B	<i>Epic – Kitchens</i>		67.4	73.0	67.1	54.1

444 D Domain Generalization

445 Domain generalisation aims to build a predictor that can perform well in an unseen test domain,
446 known as out-of-distribution generalisation. The main objective of this experiment is to learning
447 video representations that transfer well to a novel previously unseen dataset. We take the MOFO
448 and non-MOFO pretrained models that have already learned features from one dataset and finetune
449 them to adapt them to a new dataset. Results in Table ?? show that our proposed MOFO model
450 and non-MOFO pretrained model got on-par results; our MOFO pretrained model’s accuracy on
451 SSV2 is marginally higher when pretraining is done on Epic-Kitchens, and marginally worse on
452 Epic-Kitchens when pretraining is done on SSV2. These results have inspired me to design a self-
453 supervision task to enhance generalisation.

454 E Automatic Motion Area Detection

455 **Automatic vs. supervised motion area detection.** We compare the results using our automatically
456 detected motion areas and the ground truth bounding box annotation provided by Damen et al.



(a)

Method	Annotation	Epic-Kitchens
		Verb Top-1
MOFO supervision	Supervised	73.26
	Automatic(ours)	72.99

(b)

Figure 7: (a) Comparison between the unsupervised and supervised motion area detection, **green** rectangles indicate the unsupervised while **red** ones show supervised detected motion area. (b) Effect of supervised vs. automatic motion area utilisation in MOFO.

457 [2022] on the Epic-Kitchens dataset in Table 7(b). Our automatic motion detection results are close
 458 compared to supervised annotations, as seen in Table 7(b), despite the challenging camera motion
 459 from the egocentric videos.

460 We compute the Intersection over the Union (IoU) metric to compare our automatic detector with
 461 the supervised annotated bounding boxes on both datasets Damen et al. [2022], Materzynska et al.
 462 [2020]. For the Epic-Kitchens dataset, the IoU is 40%, and for Something-Something V2,
 463 the IoU is 31%. Although these numbers are lower, our automatic motion detection only detects motion
 464 and ignores unnecessary static objects near the motion. As you can see in Fig. 7(a), our automatic
 465 motion box still focuses on the area and object of interest, which is the key requirement.

466 In Fig. 8, we present additional qualitative examples of our automatic motion area detection com-
 467 pared with the provided supervised annotation for Epic-Kitchens and Something-Something V2
 468 datasets. These samples show that our proposed automatic motion area detection minimises the
 469 impact of the static object in the motion box while highlighting the motion areas. Our automatic
 470 motion box concentrates on the area and item of interest, which is necessary for our proposed approach,
 471 even for self-supervision or finetuning.

F Related Work

473 Self-supervised learning (SSL) is a developing machine learning technique that has the potential to
 474 address the issues brought about by over-dependence on labelled data. High-quality labelled data
 475 have been essential for many years to develop intelligent systems using machine learning techniques.
 476 Consequently, high-quality annotated data costs are a significant bottleneck in the training process.
 477 Grow the research and development of generic AI systems at an inexpensive cost. Self-learning
 478 mechanisms with unstructured data are one of the top focuses of AI researchers. Collecting and la-
 479 belling a wide range of diverse data is almost impossible. Researchers are developing self-supervised
 480 learning (SSL) methods that can pick up on fine details in data to address this issue. The introduction
 481 to self-supervised learning in video understanding is followed by a review of the literature on video
 482 action recognition, the downstream task we have recently focused on.

F.1 Self-supervised Video Representation learning

484 The effectiveness of deep learning-based computer vision relies on the availability of a considerable
 485 amount of annotated data, which is time-consuming and expensive to obtain. Supervised learning
 486 is trained over a given task with a large, manually labelled dataset. In addition to the costly manual
 487 labelling, generalisation mistakes and erroneous correlations are other problems with supervised
 488 learning.

489 Large labelled datasets are difficult to create in particular situations, making it challenging to con-
 490 struct computer vision algorithms. Most computer vision applications in the real world use visual
 491 categories not included in a common benchmark dataset. In specific applications, visual categories
 492 or their appearance are dynamic and vary over time. Therefore, self-supervised learning could be

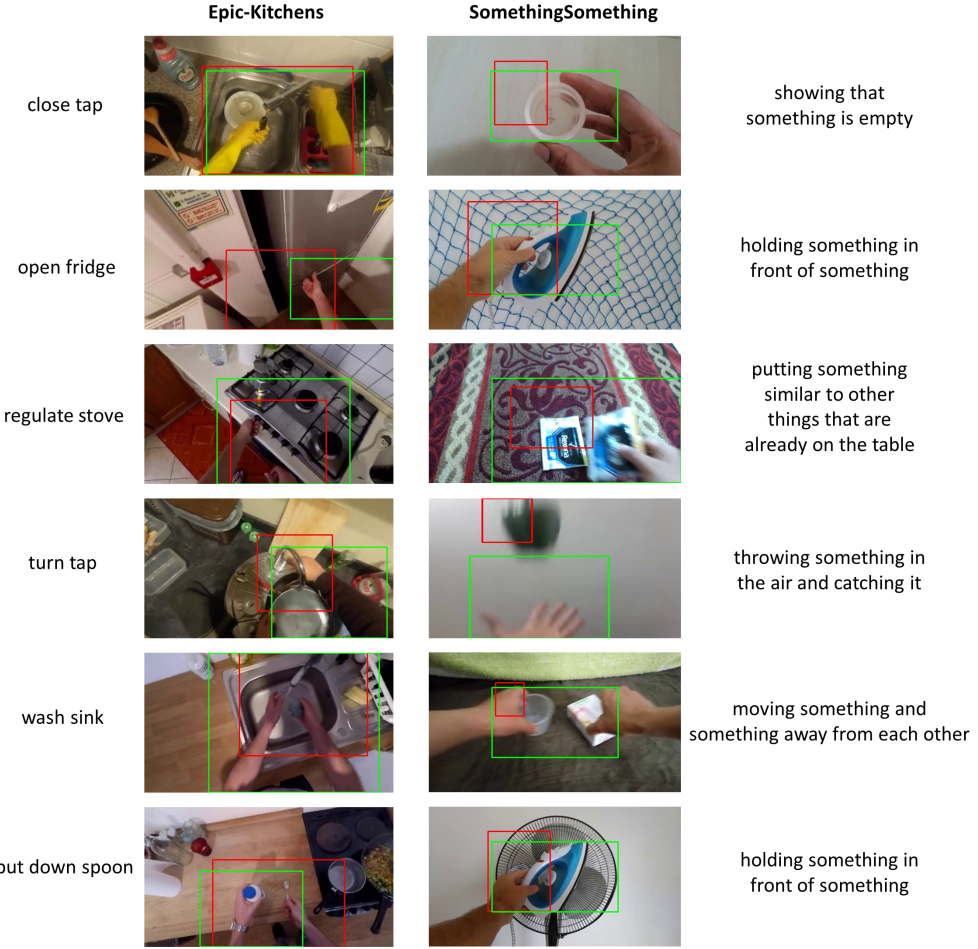


Figure 8: Comparison between the unsupervised and supervised motion area detection, **green** rectangles indicate the unsupervised while **red** ones show supervised detected motion area.

493 created that uses a limited number of labelled examples to learn to recognise new concepts effec-
 494 tively. A substantial research effort focuses on learning from unlabeled data, which is much easier
 495 to acquire in real-world applications. The ultimate goal is to make it possible for machines to com-
 496 prehend new concepts quickly after only viewing a few labelled instances, similar to how quickly
 497 humans can learn.

498 SSL has gained considerable popularity since its introduction in natural language processing Devlin
 499 et al. [2019] and computer vision Doersch et al. [2015], Chen et al. [2020], Xie et al. [2020] owing to
 500 its ability to learn effective data representations without requiring manual labels. Acquiring detailed
 501 manual labels is arguably more difficult (and often expensive) in many image and video-related
 502 tasks, which makes SSL an increasingly popular paradigm in video analysis.

503 The goal of video self-supervised learning for computer vision is to learn meaningful video repre-
 504 sentations without explicit supervision, and the model trains itself to learn one part of the input from
 505 another part of the input. Self-supervised learning algorithms can learn representations by solving
 506 pretext tasks that can be formulated using only unlabeled data. These auxiliary tasks can guide the
 507 model to learn intermediate representations of data. By solving these tasks, the model learns to
 508 extract relevant features from the input data and understand the underlying structural meaning ben-
 509 efitical for practical downstream tasks. Based on the surrogate task employed, the training objective
 510 for self-supervised learning is defined, and model parameters are updated through gradient descent
 511 to minimise prediction error. Therefore, models are trained to solve these pretext tasks. As a result,
 512 they learn to capture meaningful and useful representations that can be used for various downstream
 513 video understanding tasks, such as video action recognition F .2.

514 Video-based self-supervised learning techniques start from image tasks. Several specifically de-
515 signed tasks, including image inpainting Pathak et al. [2016], solving jigsaw puzzles Noroozi and
516 Favaro [2016], and image colour channel prediction Zhang et al. [2016] are proposed to learn image
517 features. SSL has recently yielded successful results in learning visual representations from unla-
518 beled videos with various pretext tasks Yun et al. [2022], Caron et al. [2021], Gupta et al. [2022].
519 These methods use a backbone that has been pretrained with images or videos in a self-supervised
520 manner to perform tasks on videos, including contrastive learning Yun et al. [2022], Guo et al.
521 [2022], Yang et al. [2020], self-distillation Caron et al. [2021], or Masked Modeling which selects
522 a random section of the input sequence to mask out, and then predicts the features of those sec-
523 tions Wei et al. [2022], Gupta et al. [2022], Tong et al. [2022], Girdhar et al. [2022a]. Many existing
524 works Fernando et al. [2017], Xu et al. [2019], Wang et al. [2020a] have been proposed to focus on
525 temporal information, such as making models sensitive to the temporal differences of input data.

526 As mentioned before, earlier works build on a concept of self-supervision by taking RGB frames as
527 input to learning to predict action concepts Wang and Koniusz [2021], using Convolutional Neural
528 Networks (CNNs) models to use frame-wise features and average pooling Karpathy et al. [2014] dis-
529 carding the temporal order. Thus, frame-wise CNN scores were fed to LSTMs Donahue et al. [2015]
530 while in two-stream networks Simonyan and Zisserman [2014], representations are computed for
531 each RGB frame and every ten stacked optical flow frames. Spatio-temporal 3D CNN filters Tran
532 et al. [2015], Varol et al. [2017], Feichtenhofer et al. [2017], Carreira and Zisserman [2017] model
533 spatio-temporal patterns. Persistence of Appearance, a motion cue proposed by PAN Zhang et al.
534 [2019], allows the network to extract the motion information from adjacent RGB frames directly.
535 Vision Transformers (ViTs) Dosovitskiy et al. [2020], Khan et al. [2022] have emerged as an ef-
536 fective alternative to traditional CNNs. The architecture of Vision Transformer is inspired by the
537 prominent Transformer encoder Devlin et al. [2018], Vaswani et al. [2017] used in natural language
538 processing (NLP) tasks, which process data in the form of a sequence of vectors or tokens. Like the
539 word tokens in NLP Transformer, ViT generally divides the image into a grid of non-overlapping
540 patches before sending them to a linear projection layer to adjust the token dimensionality. Feed-
541 forward and multi-headed self-attention layers are then used to process these tokens. ViTs have a
542 wide range of applications in numerous tasks due to their capacity to capture global structure through
543 self-attention, such as classification Zhang et al. [2021], Xiong et al. [2022], Li et al. [2022b], object
544 detection Chen et al. [2022], Li et al. [2022c], segmentation Choudhury et al. [2022], Caron et al.
545 [2021], Baldassarre and Azizpour [2022] and retrieval Gabeur et al. [2020].

546 Inspired by ViT Dosovitskiy et al. [2020], ViViT Arnab et al. [2021] and Timesformer Bertasius et al.
547 [2021] were the first two works that successfully implemented a pure transformer architecture for
548 video classification, improving upon the state of the art previously set by 3D CNNs. In these models,
549 the video clip of RGB frames is embedded into 3D patches to produce downsampled feature maps.
550 Then, these encoded 3D patches are encoded by a Video Transformer Patrick et al. [2021], Zhang
551 et al. [2022]. In the following work, Arnab et al. [2021] defines the tubelet embedding tokenisation
552 method and inspired some other works to represent a video input by extracting non-overlapping,
553 spatiotemporal tubes to propose their method Yan et al. [2022].

554 In another line of research, Masked Autoencoders (MAEs) have recently been demonstrated to be
555 powerful yet conceptually simple and efficient and have proven an effective pretraining paradigm
556 for Transformer models of text Devlin et al. [2018], images He et al. [2022], and, more recently,
557 videos Tong et al. [2022]. The learnt self-supervised model from the pretext task can be applied to
558 any downstream computer vision tasks, including classification, segmentation, detection, etc.

559 Nowadays, encoder-decoder Transformer-based architectures are commonly used in self-supervised
560 learning for video representation learning. These architectures take advantage of the Transformer
561 models' strengths, initially created for natural language processing challenges, and adapt them to
562 process and comprehend video data. In the context of video representation learning, the encoder-
563 decoder Transformer architecture typically consists of the following components:

- 564 1. **Encoder** The encoder processes the input video data and generates a condensed represen-
565 tation of the video. Each video frame or 3D tablets is typically treated as a sequence of
566 features to be input into the Transformer encoder. Multiple layers of self-attentional and
567 feed-forward neural networks can be used in the encoder to capture the video's temporal
568 dependencies, spatial relationships, and long-range dependencies.
- 569 2. **Decoder:** Based on the self-supervised task, the decoder generates a prediction using the
570 encoder's learnt representation. The decoder must solve the surrogate task used for self-

571 supervised learning. For instance, if the self-supervised objective is to anticipate the tem-
572 poral order of shuffled frames, the decoder may correctly predict that order.

573 In transformer-based architecture, the self-attention mechanism powers both the encoder and de-
574 coder. Self-attention architectures typically are made up of a series of transformer blocks. Each
575 transformer block consists of two sublayers: a feed-forward layer and a multi-head self-attention
576 layer. An input is divided into patches, and attention evaluates each 3D input patch's usefulness be-
577 fore drawing on it to produce the output. The Transformer's self-attention mechanism lets the model
578 focus on different parts of the video frames while considering their dependencies. Therefore, con-
579 sidering their relative importance, it draws from each input component to produce the output. The
580 query(Q), key(K), and value(V) vectors are the three sets of calculated vectors in the transformer
581 architecture. These are determined by multiplying the input by a linear transformation.

582 F .2 Video Action Recognition

583 Although it is simple for humans to recognise and categorise actions in video, automating this
584 process is challenging. Human action recognition in video is of interest for applications such as
585 automated surveillance Khan et al. [2020] detecting anomalies in a cameras field of view that has at-
586 tracted attention from vision researchers Vaswani et al. [2005], elderly behaviour monitoring Sarkar
587 et al. [2005], human-computer interaction, content-based video retrieval Sowmyayani and Rani
588 [2022], and video summarization Shabani et al. [2011]. Activity analysis must be able to iden-
589 tify atomic movements like "walking," "bending," and "falling" on their own while monitoring the
590 daily activities of elderly people, for instance Shabani et al. [2010]. Therefore, action recognition is
591 a challenging problem with many potential applications.

592 **Action Recognition Datasets** Human action recognition aims to understand human activities oc-
593 curring in a video as humans can understand. While some simple actions, like standing, can be
594 recognised from a single frame (image), most human actions are much more complex and occur
595 over a more extended period. Therefore, they must be observed through consecutive frames (video).
596 To assist organisations in understanding real-time action and dynamic, organic movement, AI/ML
597 models use human actiondatasets.

598 Something-Something V2 Goyal et al. [2017] This publically available dataset is an extensive collec-
599 tion of human-object interaction of densely labelled 174 video sequences. The dataset was created
600 by many crowd workers performing pre-trained daily humanobject interaction physical activities;
601 220,847 videos and JPG images have variable spatial resolutions and lengths.

602 Egocentric vision, sometimes known as first-person vision, is a sub-field of computer vision that
603 deals with analysing images and videos captured by a wearable camera, often worn on the head or
604 the chest and thus naturally approximates the wearer's visual field. The idea of using egocentric
605 videos has recently been utilised thanks to novel, lightweight and affordable devices such as GoPro
606 and similars Núñez-Marcos et al. [2022]. As a fundamental problem in egocentric vision, one of
607 the tasks of egocentric action recognition aims to recognise the actions of the camera wearers from
608 egocentric videos. This community did not have an extensive dataset to be used for pertaining
609 or to have a standard dataset for benchmarking until the appearance of the Epic-Kitchens Damen
610 et al. [2018, 2020a,b], the largest and most complete egocentric dataset contains 97 verb classes,
611 300 noun classes and 3806 action classes. Understanding egocentric videos requires detecting the
612 actor's movement and the object with which the actor interacts.

613 Several existing methods leveraged object detection to improve egocentric video recognition Wang
614 et al. [2020b,b], Wu et al. [2019], Ma et al. [2016], among which Wu et al. [2019] also incorporate
615 temporal contexts to help understand the ongoing action. These approaches may have limited uses in
616 real-world systems since they demand time-consuming, labour-intensive item detection annotations
617 and are computationally expensive. In contrast, our framework does not depend on costly object
618 detectors. Recently, Shanetal.Shan et al. [2020] developed a hand-object detector to locate the active
619 object. When the detector is well-trained, it can be deployed on the target dataset; however, running
620 it on high-resolution frames still costs far more than using our method.

621 **Motion in Action Recognition:** Motion cuesAkar et al. [2022], Wang et al. [2019], Li et al. [2021]
622 have been recognised as necessary for video understanding in the past few years. Most works use
623 optical flow, a motion representation component in many video recognition techniques, to obtain

624 the statistical motion labels required for their work Yang et al. [2021], separating the background
625 from the main objects in optical flow frames. Optical flow is the pattern of visible motion of objects
626 and edges and helps calculate the motion vector of every pixel in a video frame. Optical flow is
627 widely used in many video processing applications as a motion representation feature that can give
628 important information about the spatial arrangement of the objects viewed and the rate of change of
629 this arrangement. Optical flow-based techniques are sensitive to camera motion since they capture
630 absolute movement. Optical flow computation is one of the fundamental tasks in computer vision.
631 In practice, the flow has been helpful for a wide range of problems, for example, pose estimation
632 Pfister et al. [2015], representation learning Senturk et al. [2022], segmentation Luiten et al. [2020],
633 and even utilised as a tracking substitute for visual signals (RGB images) Sidenbladh et al. [2000].
634 Since optical flow can capture continuous or smoothly varying motion, such as motion caused by
635 a change in camera view, it is not a good idea to use it to detect a change in salient objects. To
636 build pixel-level representations from raw high-resolution videos with complex scenes, Xiong et al.
637 [2021] proposes a self-supervised representation learning framework based on a flow equivariance
638 objective. This representation is beneficial for object detection. In another work Li et al. [2019], a
639 multi-task motion-guided video salient object detection network is proposed consisting of two sub-
640 networks. One sub-network is used to detect salient objects in still images, and the other is used to
641 detect motion saliency in optical flow images. Most motion descriptors use absolute motions and
642 thus only work well when the camera and background are relatively static, such as Fleet & Jepson's
643 phase-based features Fleet and Jepson [1993] and Viola et al.'s generalised wavelet features Viola
644 et al. [2005]. Therefore, the critical problem is identifying characteristics that accurately capture the
645 motion of hands or objects while impervious to the camera and backdrop motion.

646 Relying only on optical flow to capture the motion is not a robust solution as it is heavily affected
647 by camera motion. To mitigate this problem, Wang et al. [2019] presented a self-supervised spatiotemporal
648 video representation by predicting a set of statistical labels derived from motion and
649 appearance statistics using extracting optical flow across each frame and two motion boundaries
650 Dalal et al. [2006] which are obtained by computing gradients separately on the horizontal and
651 vertical components of the optical flow.

652 In another line of work, masked autoencoder models have been proposed to learn underlying data
653 distribution in a self-supervised manner without explicitly focusing on motion Tong et al. [2022].
654 Even though this model can perform spatiotemporal reasoning over content, the encoder backbone
655 could be more effective in capturing motion representations. The critical contribution of our work
656 is explicitly imposing motion information in both SSL phases in the self-supervised pretext training
657 without human annotations and then in the finetuning stage, besides introducing an automatic motion
658 detection to detect salient objects and motion in the video without the overhead and limitation of a
659 pretrained and annotated object detector.